Evaluation of HZETRN on the Martian Surface: Sensitivity tests and model results

Tony C. Slaba[a], Nicholas N. Stoffle[b]

[a]NASA Langley Research Center, Hampton VA 23681 USA
[b]Leidos, Houston, TX 77004 USA

Abstract

The Mars Science Laboratory Radiation Assessment Detector (MSLRAD) is providing continuous measurements of dose, dose equivalent, and particle flux on the surface of Mars. These measurements have been highly useful in validating environmental and radiation transport models that will be heavily relied upon for future deep space missions. In this work, the HZETRN code is utilized to estimate radiation quantities of interest on the Martian surface. A description of the modeling approach used with HZETRN is given along with the various input models and parameters used to define the galactic cosmic ray (GCR) environment and Martian geometry. Sensitivity tests are performed to gauge the impact of varying several input factors on quantities being compared to MSLRAD data. Results from these tests provide context for inter-code comparisons presented in a companion paper within this issue. It is found that details of the regolith and atmospheric composition have a minimal impact on surface flux, dose, and dose equivalent. Details of the density variation within the atmosphere and uncertainties associated with specifying the vertical atmospheric thickness are also found to have minimal impact. Two widely used GCR models are used as input into HZETRN and it is found that the associated surface quantities are within several percent of each other.

Keywords

Mars; Curiosity; MSLRAD; space radiation; HZETRN; Geant4; FLUKA; PHITS; MCNP6

Introduction

For future missions to Mars, models will be heavily relied upon to quantify expected radiation levels within complicated shielding geometries during transit and on the planetary surface. It is therefore prudent to continuously verify and validate such models to improve uncertainty assessments and gain insight into possible systematic model errors. Several models have already been compared to measurements from the Mars Science Laboratory Radiation Assessment Detector (MSLRAD) obtained in-transit to Mars (Zeitlin et al., 2013) and on the surface (Matthia et al., 2016). It has been generally found that the models are in reasonable agreement with MSLRAD measurement data if integrated quantities such as dose or dose equivalent are considered (Zeitlin et al., 2013; Matthia et al., 2016).

Although such comparisons are highly useful in providing a simple and relevant measure of model uncertainty, integrated exposure quantities can obscure certain details. For example, the recent work of Matthia et al. (2016) showed that Monte Carlo (MC) simulation codes and the deterministic code HZETRN vary widely in the prediction of secondary light ion (^{2}H, ^{3}H, ^{3}He) spectra over the full energy range of interest to space applications (~1 MeV/n up to 10^{5} MeV/n). The proton and ^{4}He energy spectra computed with the codes were in excellent agreement above ~500 MeV/n, where transport results are dominated by primary galactic cosmic ray (GCR) ions and influenced mainly by total nuclear cross sections and atomic stopping powers having relatively small uncertainties (Tai et al., 1997; Sihver et al., 2012). However, at lower energies measured by MSLRAD (less than ~100 MeV/n), where nuclear production makes a significant contribution to observed particle spectra, the codes showed larger variation and uncertainty. Such differences may be important to fluence-based risk assessment models (Cucinotta et al., 2013) and pertinent biological responses such as cardiovascular disease and central nervous system detriment.

Although the comparisons between MSLRAD data and various models published to date generally show that the models are capable of providing reliable assessments of the radiation environment on the Martian surface, further improvements and continued validation and uncertainty quantification efforts are still needed. Such efforts inevitably lead to improved models with reduced uncertainties, thereby leading to more optimal vehicle and habitat designs with reduced exposure, mass, and cost. As discussed in the summary paper for this special issue (Hassler et al., 2017), a workshop was held in Boulder, CO in June 2016 with the purpose of comparing widely used transport codes to new and unpublished MSLRAD data that were not available to the modeling teams. Only certain input parameters, boundary conditions, and output requirements were specified prior to the workshop as discussed by Hassler et al. (2017). This type of independent or "blind" validation effort is highly useful and informative and has the advantage of removing unintentional bias or ad-hoc empirical adjustments from model results.

In this work, the modeling approach used to evaluate HZETRN in this set of comparisons is described. A brief summary of HZETRN is provided, along with a description of the geometry and boundary condition specification. A complete set of input models and parameters used to generate the HZETRN results compared to MSLRAD data in Matthia et al. (2017) are provided in the Appendix. Notably, although certain input parameters and conditions were specified to the modeling teams prior to the workshop, other components needed to perform the

relevant calculations were intentionally left unspecified. For example, each team was free to choose a model to describe the primary GCR particle spectra, atmosphere and regolith composition, and other related factors. Leveraging the high degree of computational efficiency associated with HZETRN, sensitivity tests were also performed to determine to what extent some of the unspecified factors influence quantities of interest on the Martian surface. Results of these tests are useful in providing context for the summary comparison paper of Matthia et al. (2017) contained within this issue so that variation between codes and differences against MSLRAD data can be more clearly interpreted.

Model Overview

HZETRN

HZETRN (Wilson et al., 1991, 2016; Slaba et al., 2016) is a deterministic transport code providing numerical solutions to the time-independent, linear Boltzmann equation (Wilson et al., 1991). The transport formalism allows for a converging sequence of physical approximations to be considered, allowing highly efficient computational procedures to be implemented. Typical run times for full GCR calculations range from seconds to minutes on a single CPU. The version of the code used herein utilizes a bi-directional transport approach for neutrons and light ions (Slaba et al., 2010), allowing back-scattered albedo neutron contributions to be represented. Heavier ions are treated within the straight-ahead approximation (Wilson et al., 1991), as are the pion, muon, and electromagnetic cascade components (Norman et al., 2013). Recent improvements to the code include more detailed 3D corrections for neutrons and light ions (Wilson et al., 2016), which were not included here but may be considered in future work. The NUCFRG3 (Adamczyk et al., 2012) model is used for describing nuclear fragmentation of heavy ions. Light ion and neutron interaction models are described elsewhere (Wilson et al., 1991; Cucinotta, 1993; Cucinotta et al., 1996). The most recent version of the code, capable of reproducing the results presented herein, is HZETRN2015 and can be obtained through the website: https://software.nasa.gov. A web-based tool utilizing HZETRN2015 with additional capabilities for specifying geometry, boundary conditions, and response functions is also available at https://oltaris.nasa.gov.

Geometry setup

The implementation of HZETRN for Mars surface calculations considers the atmospheric geometry and variable density profile in a ray-by-ray computational procedure as described by Slaba et al. (2013). As shown on the left side of Figure 1, the geometry is defined by a regolith sphere with a radius of 3396.2 km (average Mars radius) surrounded by a spherical shell representing the Martian atmosphere. A target point is placed on the surface at the interface between the atmosphere and regolith. Although not shown in the figure, the GCR boundary condition is assumed to impinge isotropically on the sphere.

In order to couple this geometry to HZETRN within the bi-directional transport formalism, ray-tracing procedures are utilized. First, incoming GCR ions impinging from below the horizon are assumed to be fully blocked by the Martian surface and are therefore neglected (i.e., they are assumed to make no contribution to the exposure on the surface). For GCR ions impinging from the remaining upper 2π solid angle, the ray-trace path length through the atmosphere is needed for transport calculations and may be computed if the vertical thickness is known (see right side of Figure 1 and geometric relationships from Simonsen et al. (1990)). Simple extensions to the basic geometric relationships have been incorporated so that density variations occurring along the ray-trace path can be computed, thereby allowing pion and muon decay rates to be properly evaluated. To improve computational efficiency, a constant thickness of 300 g/cm^2 was assumed for all path lengths through the regolith sphere. This thickness has been found to be sufficiently large to reach equilibrium in the albedo neutron field without unnecessarily increasing computational cost in transport calculations.

These ray-trace procedures are performed prior to transport code execution over a large number of rays ($\sim 10^3$) each of which account for the same fraction of the full solid angle. In general, the ray-by-ray transport calculation becomes a series of slab calculations with a target point placed between an atmosphere shield with varying density and backed by 300 g/cm^2 of regolith. Precise definitions of the atmosphere composition, regolith composition, vertical thickness, and density profile along the vertical ray are discussed later in this report in the context of sensitivity studies.

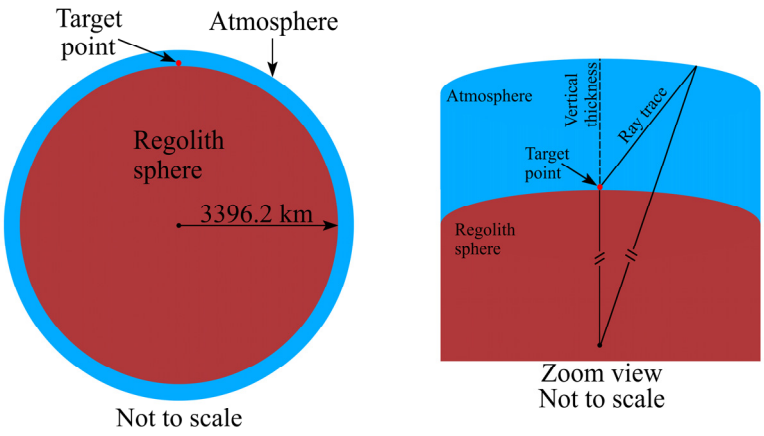

Figure 1. Mars surface geometry in full view (left) and zoom view (right).

Sensitivity Tests

As discussed by Hassler et al. (2017), only certain input conditions were precisely specified to the modeling teams. These fixed conditions were:

- the dates over which the measurements were taken (November 15, 2015 – January 15, 2016),
- the location of MSLRAD during the measurement period (137.4° east, -4.7° south),
- the altitude of MSLRAD during the measurement period (-4.431 km),
- the vertical atmospheric thickness during the measurement period (23 g/cm^2).

Other factors that can impact computed exposure quantities on the surface were left unspecified and could therefore be freely chosen by the individual modeling teams. The complete set of input specifications used for HZETRN comparisons to MSLRAD data are provided in the Appendix. In this section, the impact of specifying the regolith composition, atmosphere composition, vertical density profile, and GCR boundary condition on radiation quantities computed on the surface is quantified.

Regolith and atmospheric compositions considered herein are given in Tables 1 and 2, respectively. The regolith compositions used in this work were provided in McKenna-Lawlor et al. (2012) and represent compositions for three possible Mars landing sites studied in their paper. The column labeled Default$_{Reg}$ is the global average from McKenna-Lawlor et al. (2012) and is expected to be most applicable to the MSLRAD comparison. The Phoenix regolith definition contains a high concentration of water (ice) and is being assessed here as a bounding case. The atmosphere composition labeled as Default$_{Atm}$ was provided in De Angelis et al. (2004). The simplified CO_2 composition was also considered here since it was utilized by some of the MC codes in this validation effort. The Default$_{Reg}$ and Default$_{Atm}$ compositions were used in the final model results compared to MSLRAD data and are the same compositions utilized by the OLTARIS website (Singleterry et al., 2011) described in the introduction.

For the vertical density profile, two Martian atmospheric models (Mars Climate Database (MCD) version 4.3 (Millour et al., 2008) and Mars-GRAM 2001 (Justus and Johnson, 2001)) were evaluated with the constraint that the vertical thickness of 23 g/cm^2 be maintained. Finally, for the GCR boundary condition, two models (Badhwar-O'Neill 2014 (BON2014) (O'Neill et al., 2015) and DLR2013 (Matthia et al., 2013)) were evaluated using the dates specified earlier in this section. The MCD atmosphere model and BON2014 GCR model were used in the final model results compared to MSLRAD data [Matthia et al. 2017]. Additional calculations were also performed in this sensitivity analysis to determine how perturbations to the vertical thickness and solar activity would affect output quantities.

It should be noted that the Default$_{Reg}$ regolith definition, Default$_{Atm}$ atmosphere definition, BON2014 GCR model, and MCD atmosphere model were taken as the baseline definitions, and results from those combinations of models and inputs were used in the final comparison to MSLRAD data. For the sensitivity test results presented in this section, a single input condition was varied while all other baseline definitions were held fixed. For example, in the case of the Martian regolith, all four definitions in Table 1 were evaluated separately with the baseline definitions of the atmosphere composition, GCR model, and atmosphere model.

Table 1. Mass percentages of Martian regolith used in sensitivity tests (McKenna-Lawlor et al., 2012).

Compound	$Default_{Reg}$	Viking 1	Phoenix	Mawrth Vallis
SiO_2	51.2	48.4	27.0	55.0
Fe_2O_3	9.3	15.7	4.0	38.0
Bulk $Al_2MgCaNa_2K_2O_7$	32.1	32.1	19.0	0.0
H_2O	7.4	3.8	50.0	7.0

Table 2. Mass percentages of Martian atmosphere used in sensitivity tests (De Angelis et al., 2004).

Compound	$Default_{Atm}$	Simple
CO_2	95.482	100
N_2	2.705	0
Ar	1.603	0
O_2	0.130	0
CO	0.080	0

Figure 2 and Table 3 provide results obtained by varying the regolith composition as defined previously in Table 1. As would be expected, Figure 2 shows that the neutron field above ~100 MeV is insensitive to the regolith composition since most of these particles are produced in the forward direction from GCR protons and heavier ions suffering nuclear collisions in the atmosphere above the surface. Below ~100 MeV, the field becomes increasingly isotropic and roughly half of the neutrons are produced in the regolith and ejected back into the atmosphere. The plots suggest that changes to the material composition have little impact on the surface spectrum even at low energies except in the case of the Phoenix landing site result. In this case, the significant increase in water compared to the other sites greatly attenuates the low energy neutron field due to the large energy transfers associated with neutron-hydrogen elastic collisions. As stated earlier in this section, the Phoenix definition was considered as a bounding case to show the impact of high water content on the surface neutron flux. The result is less relevant to the MSLRAD comparison where the surface water content is known to be much lower.

For a quantitative assessment, and as a reference for comparison to integrated quantities, it is helpful to note that for moderate shielding in free space, neutrons below 1 MeV account for <10% of the neutron effective dose (Heilbronn et al., 2015) and consequently make an even smaller contribution to the total exposure. This indicates that spectral differences shown in Figure 2 at the lowest energies are of less concern to integrated exposure quantities. Between 1 MeV and 10 MeV, spectral variation in Figure 2 between the relevant regolith definitions ($Default_{Reg}$, Viking 1, and Mawrth Vallis) is within $\pm$10%. Further quantitative assessments can be found in Table 3 where the variation on dose, dose equivalent, and neutron effective dose is clearly small.

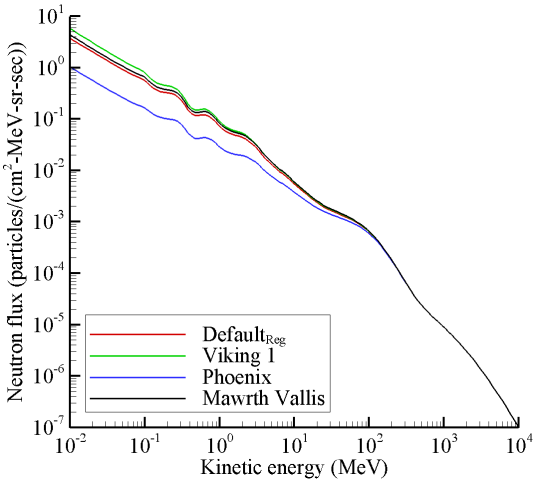

Figure 2. Neutron flux on the Martian surface using regolith definitions from Table 1.

Table 3. Integrated exposure quantities on the Martian surface using regolith definitions from Table 1.

Regolith definition	Dose in tissue (mGy/day)	Dose equivalent (mSv/day)	[1]Neutron effective dose (mSv/day)
$Default_{Reg}$	0.172	0.539	0.163
Viking 1	0.174	0.579	0.176
Phoenix	0.167	0.452	0.124
Mawrth Vallis	0.173	0.563	0.174

[1]The neutron effective dose column was obtained by folding the neutron spectra from Figure 2 with isotropic neutron fluence to effective dose conversion coefficients from Pelliccioni (2000).

Figure 3 shows results obtained by varying the atmosphere composition as defined previously in Table 2. In this case, surface fluxes for neutrons, protons, ^{4}He, and $Z = 14$ ions obtained using the $Default_{Atm}$ and simplified CO_2 atmosphere composition are nearly identical, indicating that atmospheric composition has a negligible impact on flux across the full energy domain. Differences on dose and dose equivalent caused by varying the atmospheric composition were found to be less than 0.3% and are therefore not shown.

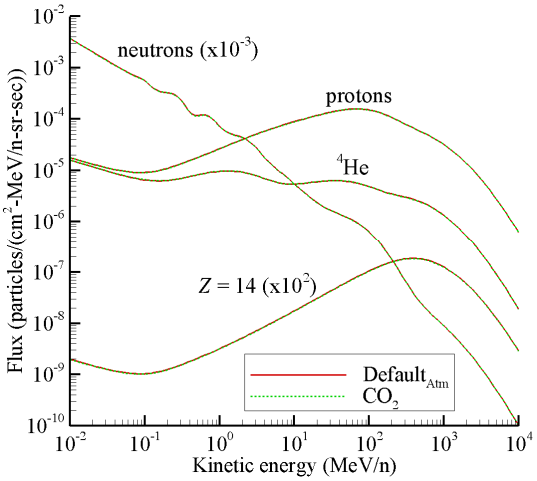

Figure 3. Charged particle fluxes on the Martian surface using the atmosphere definitions from Table 2. The neutron and $Z = 14$ flux results have been scaled by 10^{-3} and 10^2, respectively, to improve plot clarity.

Figure 4 shows results obtained by varying the model used to generate the vertical density profile. In both cases, the total vertical thickness was held fixed at 23 g/cm^2, so that the only difference being shown is associated with density variation as a function of altitude above the surface. As a result, negligible differences in the neutron and ion fields would be expected, but some impact may be seen on the electron (e^-), positron (e^+), pion ($\pi^\pm$), and muon ($\mu^\pm$) values as a result of differing decay characteristics in the atmosphere. Although moderate differences can be seen in the $\pi^\pm$ and $\mu^\pm$ fluxes, the $e^\pm$ fluxes are barely modified. The $e^\pm$ in Figure 4 are generated mainly by high energy photons emitted from the decay of neutral pions (π^0) that are produced in nuclear collisions between GCR ions and atmospheric nuclei. These neutral pions decay almost instantaneously (~10^{-17} sec), and therefore, details of the atmospheric density profile have minimal impact. Differences on dose and dose equivalent caused by varying the density profile were found to be less than 0.3% and therefore are not shown.

Figure 5 and Table 4 show the results obtained by varying the model used to generate the free space GCR spectrum impinging on the atmosphere. Previous studies (Mrigakshi et al., 2012; Slaba et al., 2014) have compared an older version of the BON model (O'Neill, 2010) to the DLR2013 model and it was found that although some moderate spectral differences exist, such differences do not have a substantial impact on integrated exposure quantities behind moderate shielding. More recent updates to the BON model, leading to BON2014 (O'Neill et al., 2015) included further comparisons between DLR2013 and BON2014 and similar conclusions were drawn.

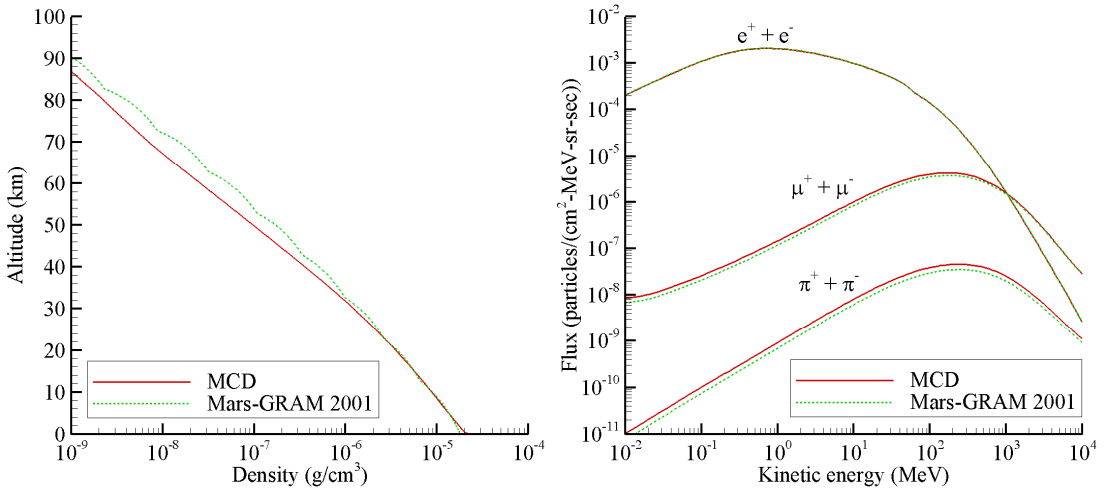

Figure 4. MCD and Mars-GRAM 2001 density profiles (left) and the corresponding electromagnetic flux components on the Martian surface (right).

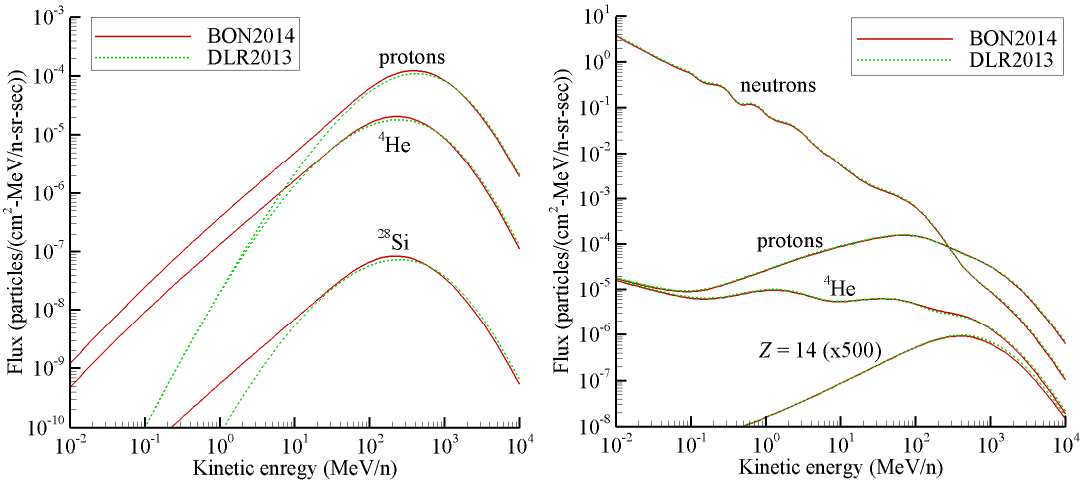

Figure 5. Selected particles from the free space GCR spectrum generated by the BON2014 and DLR2013 models (left) and related particle spectra computed on the Martian surface (right). The Z = 14 flux results have been scaled by 500 on the right plot to improve plot clarity.

Table 4. Integrated exposure quantities on the Martian surface using the BON2014 and DLR2013 GCR models.

GCR model	Dose in tissue (mGy/day)	Dose equivalent (mSv/day)
BON2014	0.172	0.539
DLR2013	0.177	0.560

The left side of Figure 5 shows the free space GCR spectrum generated by the two models for this study. Below ~50 MeV/n, the models clearly provide vastly different spectral values, yet it is known that such low energy particles make negligible contributions to exposures behind shielding (Slaba and Blattnig, 2014). At higher energies, there appears to be some minor discrepancies between the models, yet the right side of Figure 5 shows that such differences do not significantly influence surface results. Table 4 provides integrated quantities for further assessment, and it is seen that total dose and dose equivalent values vary by only 3% and 4%, respectively.

Results and discussion in this section were focused on varying some of the important input factors needed to evaluate the radiation environment on the Martian surface. In general, it was shown that variation in the regolith composition (with the exception of the hydrogenous Phoenix definition), atmosphere composition and atmospheric density profile (assuming a fixed vertical thickness of 23 g/cm^2) have minimal impact on surface exposure quantities. It was also shown that surface quantities induced by using either the BON2014 or DLR2013 models exhibited only minor differences. These sensitivity analyses are useful in providing some context for the surface results generated by various transport codes utilizing some combination of the input parameters and models considered in this study.

Uncertainty in Atmospheric Thickness and Solar Activity

In this section, further analysis is provided to gauge the impact of uncertainty associated with specifying the vertical atmospheric thickness and solar activity. While the previous section provides some context for inter-code comparisons wherein each of the codes used slightly different input parameters, this section provides some context for variation in surface quantities associated with input model/parameter uncertainty. For example, the vertical atmospheric thickness was specified for the modeling workshop as 23 g/cm^2; however, this value is not precisely known in general and carries some uncertainty. In addition, although the dates over which the measurements were collected are precisely specified and known, quantifying solar activity in terms of the solar modulation parameter for the BON2014 [O'Neill et al. 2015] model or Wolf number for the DLR2013 [Matthia et al. 2013] model carries some uncertainty as well.

The left side of Figure 6 shows the flux of selected particles on the surface using different values for the vertical atmospheric thickness. Results for the baseline value of 23 g/cm^2 are shown as the solid red line, while results for smaller and larger vertical thicknesses are shown as dashed lines. The only readily apparent differences appear in the $Z = 14$ flux and at the highest energies in the ^{4}He flux. As one might expect, the $Z = 14$ flux is larger if the vertical thickness is reduced to 20.4 g/cm^2 and smaller if the vertical thickness is increased 24.1 g/cm^2. Somewhat surprisingly, however, there appears to be little impact on the proton spectrum across the entire energy domain. Table 5 provides integrated quantities using the modified vertical atmospheric thicknesses, and it is found that the impact on dose and dose equivalent is within 3% in both cases. These results suggest that model differences observed against MSLRAD data are not heavily influenced by uncertainty in specifying the vertical atmospheric thickness.

The right side of Figure 6 shows the flux of selected particles on the surface using different values for the solar modulation parameter, ϕ, used in the BON2014 model. The baseline value computed by the model for the MSLRAD measurement dates in this study was 572 MV. To be clear, the ϕ value obtained and used in BON2014 is empirically correlated with monthly sunspot number values and is intrinsically tied to the time-delay function and other free parameters used for the local interstellar spectrum in the model (O'Neill et al., 2015). Although solar modulation values from BON2014 may appear similar to those derived from other data sources (e.g. neutron monitor or satellite data), external or independently derived values of ϕ should not be used as input into BON2014, especially for end-to-end validation studies as is being conducted here. Nonetheless, to provide some quantitative assessment of the uncertainty induced by specifying solar activity in the model, the baseline value of 572 MV was modified by $\pm$20% (likely a conservative bound (Slaba et al., 2014)). In this case, it can be seen that both charged and neutral particle spectra are noticeably changed. Larger values of ϕ correspond to a stronger solar magnetic field capable of attenuating the local interstellar spectrum and reducing the GCR intensity impinging on the Martian atmosphere. Therefore, surface fluxes appear consistently larger for smaller ϕ values, while the opposite occurs for larger ϕ values.

Table 5 shows that in this case, surface dose and dose equivalent values are modified by as much as ~20%. Based on published validation and uncertainty quantification studies with BON2014 and DLR2013 (Mrigaskhi et al., 2012; Slaba et al., 2014; O'Neill et al., 2015), one would not expect the GCR model to systematically over-predict or under-predict all particles simultaneously as occurs when ϕ is modified as in Figure 6. Moreover, past studies (Slaba et al., 2014; O'Neill et al., 2015) have shown that the GCR models are capable of predicting high energy (> 1.5 GeV) proton and alpha spectra to within measurement uncertainty. Since these high energy protons and alphas account for a large portion of the overall dose (Slaba and Blattnig, 2014) and secondary particle spectra

(Heilbronn et al., 2015) observed on the Martian surface, it is expected that model comparisons to MSLRAD data may only be moderately influenced by uncertainty in specifying solar activity parameters used in GCR models.

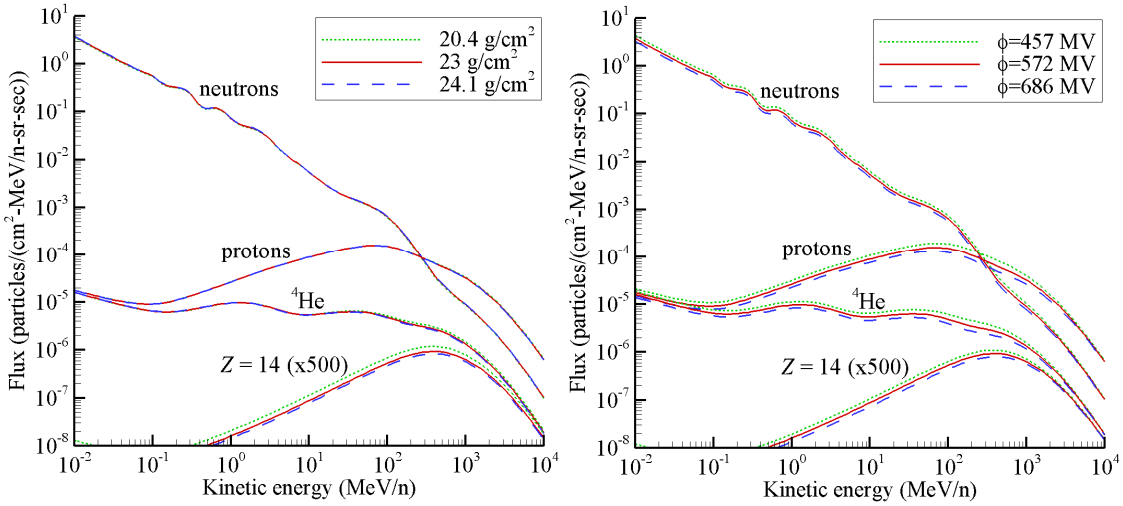

Figure 6. Particle spectra on the Martian surface using various vertical atmospheric thicknesses (left) and solar activity levels (right). The $Z = 14$ flux results have been scaled by 500 to improve plot clarity.

Table 5. Integrated exposure quantities on the Martian surface using different vertical thicknesses and solar activity levels.

Vertical thickness (g/cm^2)	Solar modulation parameter	Dose in tissue (mGy/day)	Dose equivalent (mSv/day)
20.4		0.174	0.552
23.0	572	0.172	0.539
24.1		0.171	0.535
	457	0.205	0.636
23.0	572	0.172	0.539
	686	0.147	0.467

Summary and Conclusions

This paper utilized HZETRN to compute particle flux, dose, and dose equivalent on the surface of Mars. The modeling approach coupled to HZETRN and the various input models and parameters were described. As part of a broader model verification and validation effort described within this special issue, sensitivity tests were performed to provide some context for inter-code comparisons provided in Matthia et al. (2017). It was found here that the atmosphere and regolith composition have only a minimal impact on surface quantities. Details of the density variation within the atmosphere and uncertainties associated with specifying the vertical atmospheric thickness also play a minor role. Two widely used GCR models were evaluated to provide inputs into HZETRN, and surface exposure quantities were found to be within several percent of each other. Uncertainty associated with specifying solar activity in the BON2014 GCR model was examined as well. The solar modulation parameter used within BON2014 to quantify solar activity was varied by $\pm$20% from the nominal value calculated over the MSLRAD measurement dates. Surface quantities were found to vary by as much as 20% as a result of perturbing the solar modulation parameter.

These results are important to help interpret inter-code comparisons provided in Matthia et al. (2017). In particular, it suggests that observed model-to-model differences can be attributed mainly to nuclear model uncertainty that can be reduced only with ground-based accelerator measurements of relevant cross sections and fundamental nuclear model improvements. Model-to-measurement differences can be attributed mainly to nuclear model differences and GCR model uncertainty. The latter may be reduced with additional satellite measurements in

free space and would be helpful in providing more accurate radiation assessments for both the cruise and surface components of a Mars mission.

Acknowledgements

This work was supported by the Human Research and Advanced Exploration Systems Programs under the Human Exploration and Operations Mission Directorate of NASA and by NASA contract NNJ15HK11B.

References

Adamczyk, A.M., Norman, R.B., Sriprisan, S.I., Townsend, L.W., Norbury, J.W., Blattnig, S.R., Slaba, T.C., NUCFRG3: Light ion improvements to the nuclear fragmentation model. *Nucl. Instr. Meth. Phys. A* **678**: 21-32; 2012.

Cucinotta, F.A., Calculation of cosmic ray helium transport in shielding materials. NASA TP 3354; 1993.

Cucinotta, F.A., Townsend, L.W., Wilson, J.W., Shinn, J.L., Badhwar, G.D., Dubey, R.R., Light ion components of the galactic cosmic rays: nuclear interactions and transport theory. *Adv. Space Res.* **17**: 77-86; 1996.

Cucinotta, F.A., Kim, M.Y., Chappell, L.J., Space radiation cancer risk projections and uncertainties – 2012. NASA TP 2013-217375; 2013.

De Angelis, G., Clowdsley, M.S., Singleterry, R.C., Wilson, J.W., A new Mars radiation environment model with visualization. *Adv. Space Res.* **34**: 1328-1332; 2004.

Hassler et al.,. Summary of MSLRAD workshop in LSSR special issue. Companion paper appearing in this issue; 2017.

Heilbronn, L.H., Borak, T.B., Townsend, L.W., Tsai, P.E., Burnham, C.A., McBeth, R.A., Neutron yields and effective doses produced by galactic cosmic rays interactions in shielded environments in space. *Life Sci. Space Res.* 7: 90-99; 2015.

Justus, C.G., Johnson, D.L., Mars global reference atmospheric model 2001 version (Mars-GRAM 2001). NASA TM 2001-210961; 2001.

Matthia, D., Berger, D., Mrigakshi, A.I., Reitz, G., A ready-to-use galactic cosmic ray model. *Adv. Space Res.* **51**: 329-338; 2013.

Matthia, D., Ehresmann, B., Lohf, H., Kohler, J., Zeitlin, C., Appel, J., Sato, T., Slaba, T.C., Martin, C., Berger, T., Boehm, E., Boettcher, S., Brinza, D.E., Burmeister, S., Guo, J., Hassler, D.M., Posner, A., Rafkin, S.C.R., Reitz, G., Wilson, J.W., Wimmer-Schweingruber, R.F., The Martian surface radiation environment – a comparison of models and MSL/RAD measurements. *J. Space Weather Spac.* **6**: A13; 2016.

Matthia et al.,. Summary of model results and MSLRAD data for LSSR special issue. Companion paper appearing in this issue; 2017.

Millour, E., Forget, F., Lewis, S.R., Mars climate database v4.3 detailed design document, Le Laboratoire de M´et´eorologie Dynamique. Available at http://www-mars.lmd.jussieu.fr/; 2008.

McKenna-Lawlor, S., Goncalves, P., Keating, A., Morgado, B., Heynderickx, D., Nieminen, P., Santin, G., Truscott, P., Lei, F., Foing, B., Balaz, J., Characterization of the particle radiation environment at three potential landing sites on Mars using ESA's MEREM models. *Icarus* **218**: 723-734; 2012.

Mrigakshi, A.I., Matthia, D., Berger, T., Retiz, G., Wimmer-Schweingruber, R.W., Assessment of galactic cosmic ray models. *J. Geophys. Res.* **117**: A08109; 2012.

Norman, R.B., Slaba, T.C., Blattnig, S.R., An extension of HZETRN for cosmic ray initiated electromagnetic cascades. *Adv. Space Res.* **51**: 2251-2260; 2013.

O'Neill, P.M., Badhwar-O'Neill galactic cosmic ray flux model – revised. *IEEE Trans. Nucl. Sci.*, **57**: 3148-3153; 2010.

O'Neill, P.M., Golge, S., Slaba, T.C., Badhwar-O'Neill 2014 galactic cosmic ray flux model description. NASA TP 2015-218569; 2015.

Pelliccioni M., Overview of fluence-to-effective dose and fluence-to-ambient dose equivalent conversion coefficients for high energy radiation calculated using the FLUKA code. *Radiat. Prot. Dosim.* **88**: 279-297; 2000.

Sihver, L., Lantz, M., Takechi, M., Kohama, A., Ferrari, A., Cerutti, F., Sato, T., A comparison of total reaction cross section models used in particle and heavy ion transport codes. *Adv. Space Res.* **49**: 812-819; 2012.

Simonsen, L.C., Nealy, J.E., Townsend, L.W., Wilson, J.W., Radiation exposure for manned Mars missions. NASA TP 2979; 1990.

Singleterry, R.C., Blattnig, S.R., Clowdsley, M.S., Qualls, G.D., Sandridge, C.A., Simonsen, L.C., Slaba, T.C., Walker, S.A., Badavi, F.F., Spangler, J.L., Aumann, A.R., Zapp, E.N., Rutledge, R., Lee, K., Norman, R.B., Norbury, J., OLTARIS: On-line tool for the assessment of radiation in space. *Acta Astr.* **68**: 1086-1097; 2011.

Slaba, T.C., Blattnig, S.R., Aghara, S.K., Townsend, L.W., Handler, T., Gabriel, T.A., Pinsky, L.S., Reddell, B., Coupled neutron transport for HZETRN. *Radiat. Meas.* **45**: 173-182; 2010.

Slaba, T.C., Mertens, C.J., Blattnig, S.R., Radiation shielding optimization on Mars. NASA TP 2013-217983; 2013.

Slaba, T.C. and Blattnig, S.R., GCR environmental models I: sensitivity analysis for GCR environments. *Space Weather* **12**: 217-224; 2014.

Slaba, T.C., Xu, X., Blattnig, S.R., Norman, R.B., GCR environmental models III: GCR model validation and propagated uncertainties in effective dose. *Space Weather* **12**: 233-245; 2014.

Slaba, T.C., Wilson, J.W., Badavi, F.F., Reddell, B.D., Bahadori, A.A., Solar proton exposure of an ICRU sphere within a complex structure: ray-trace geometry. *Life Sci. Space Res.* **9**: 77-83; 2016.

Tai, H., Bichsel, H., Wilson, J.W., Shinn, J.L., Cucinotta, F.A., Badavi, F.F., Comparison of stopping power and range databases for radiation transport study. NASA TP 3644; 1997.

Wilson, J.W., Townsend, L.W., Schimmerling, W., Khandelwal, G.S., Khan, F., Nealy, J.E., Cucinotta, F.A., Simonsen, L.C., Shinn, J.L., Norbury, J.W., Transport methods and interactions for space radiations. NASA RP 1257; 1991.

Wilson, J.W., Slaba, T.C., Badavi, F.F., Reddell, B.D., Bahadori, A.A., Solar proton exposure of an ICRU sphere within a complex structure: combinatorial geometry. *Life Sci. Space Res.* **9**: 69-76; 2016.

Zeitlin, C., Hassler, D.M., Cucinotta, F.A., Ehresmann, B., Wimmer-Schweingruber, R.F., Brinza, D.E., Kang, S., Weigle, G., Bottcher, S., Bohm, E., Burmeister, S., Guo, J., Kohler, J., Martin, C., Posner, A., Rafkin, S., Reitz, G., Measurements of energetic particle radiation in transit to Mars on the Mars science laboratory. *Science* **340**: 1080-1084, 2013.

Appendix

This section provides a summary of the input specifications used to run HZETRN for the comparison to MSLRAD data in Matthia et al. (2017).

- GCR model: BON2014 with input dates specified as November 15, 2015 – January 15, 2016. For reference, this yielded a solar modulation parameter of 572 MV.
- Regolith composition: See $\text{Default}_{\text{Reg}}$ definition in Table 1.
- Atmosphere composition: See $\text{Default}_{\text{Atm}}$ definition in Table 2.
- Atmospheric density model: MCD v4.3.
    - MCD v4.3 inputs: location specified as 137.4° east, -4.7° south, and the solar longitude (L_s) was selected as 137.4° to give a vertical atmospheric thickness of 23 g/cm^2.